Ion-induced electrostatic charging of ice at 15–160 K

J. Shi,[1] M. Famá,[1] B. D. Teolis,[2] and R. A. Baragiola[1,*]

[1]*University of Virginia, Laboratory for Atomic and Surface Physics, Thornton Hall, Charlottesville, Virginia 22904-4238, USA*

[2]*Southwest Research Institute, San Antonio, Texas 78227, USA*

(Received 31 August 2011; published 17 January 2012)

We studied electrostatic charging of ice films induced by the impact of 1−200-keV Ar^+ ions and their subsequent discharging postirradiation. We derived the positive surface electrostatic potential from the kinetic energy of sputtered molecular ions and with a Kelvin probe. Measurements were performed as a function of film thickness, temperature, and ion energy. Charging requires that the projectile ions are stopped in the ice and that the ice temperature is below 160 K. The decay of the electrostatic charge after irradiation is determined by two time constants, corresponding to the detrapping of trapped charges in shallow and deep traps within the ice. Amorphous solid water films are found to charge to a higher electrostatic potential than crystalline ice films. The surface potential of crystalline ice increases and decreases during cooling and warming, respectively, without hysteresis. We present a model to describe the charging and discharging processes.

DOI: 10.1103/PhysRevB.85.035424 PACS number(s): 79.20.Rf, 77.22.Jp, 34.35.+a

I. INTRODUCTION

Water ice below 160 K is ubiquitous in the cold interstellar medium and in the outer solar system, where it is subject to continuous bombardment by ionizing particles. Although some of the subsurface materials of the icy satellites are found to be electrical conductors,[1] their surfaces are primarily electrical insulators. Ion and electron implantation, together with photoelectron, secondary electron, and secondary ion emission, will often leave the icy surfaces charged. The charged icy surfaces might be capable of deflecting or even reflecting low-energy magnetospheric projectiles, so that charging might affect the current flow into the icy surfaces. The return of secondary electrons to a positively charged surface can have significant effects in the sputtering of insulators.[2] Limited laboratory studies have focused on the charging of ice films due to charge imbalance upon ion[3] or electron[4,5] injection. Other research has examined the simpler case of charging and breakdown in rare gas solids.[6–8]

In our previous report on ion-induced electrostatic charging of ice by 100 keV Ar^+,[3] we found that ice films with thicknesses greater than the maximum ionization range of the Ar^+ ions were charged to a saturation-positive surface potential, measured from the kinetic energies of sputtered H_3O^+. We found that the equilibrium or saturation surface potentials of the films depend on the ion flux and film thickness, while the time constants for charging the ice films depend only on the incident ion flux. The surface potentials were limited by the dielectric breakdown of the films above ∼100 V. We proposed a quantitative model, which considers (i) temporary charge storage in traps, (ii) later thermally induced detrapping assisted by the locally perturbed electric field from subsequently injected ions, and (iii) positive charge drift into the substrate (which occurs by electron diffusion out of the substrate).

Here, we report on experimental studies of electrostatic charging and discharging in ice films induced by 1−200-keV Ar^+ ion bombardment. We explore the charging/discharging as a function of film thickness, temperature, and ion energy.

II. EXPERIMENTAL DETAILS

A brief description of the experimental setup has been published elsewhere.[3] The experiments were conducted in an ultra-high vacuum chamber with a base pressure of $\sim 10^{-10}$ Torr. We condensed high-purity ice films by flowing pure degassed water through a collimated capillary array doser onto an electrically grounded gold-coated quartz-crystal microbalance substrate, cooled to temperatures between 40 and 150 K by a liquid helium refrigerator.[9] Upon attachment or detachment of gas molecules, the resonant frequency of the crystal changes proportionally to the deposited mass per unit area. By converting the measured frequency change into number of molecules deposited, we obtained the column density, η, of the films with a sensitivity of ∼0.04 ML (1 ML = 10^{15} molecules cm^{-2} or approximately a surface monolayer). Ice films used in this report range from 800 to 3000 ML. High energy (20−200 keV) Ar^+ beams were produced from a mass-analyzed 20−300-keV Veeco ion accelerator at 45° incident angle. Collimated low-energy (<5 keV) Ar^+ beams were produced by an NTI 1401 ion gun at 30° incident angle. Ions that penetrate the ice film lose their energy through electronic and nuclear collision before stopping in the film. The ionization range, with a roughly cosine dependence on the incident angle, can be calculated with the Monte Carlo code TRIM.[10] Both the low- and high-energy Ar^+ beams were scanned uniformly over the sample. We measured the ion beam flux, j, with a Faraday cup, and derived the fluence, $F = \int j dt$ over irradiation time t. Sputtered secondary ions emitted normal from the surface were detected with a Hiden EQS 300 secondary ion mass spectrometer (SIMS) equipped with an electrostatic energy analyzer, capable of operation with an energy resolution between 0.05 and 1 eV. The number of secondary ions is negligible compared to that of incident ions and does not affect the current measurements, within errors.

We monitored the kinetic energies of sputtered secondary ions to determine the surface potential. We chose the protonated water ion H_3O^+, the most abundant secondary ion after H^+, for a detailed energy scan. Figure 1 shows a series of energy scans measured at different irradiation times during electrostatic charging of an ice film. The peak

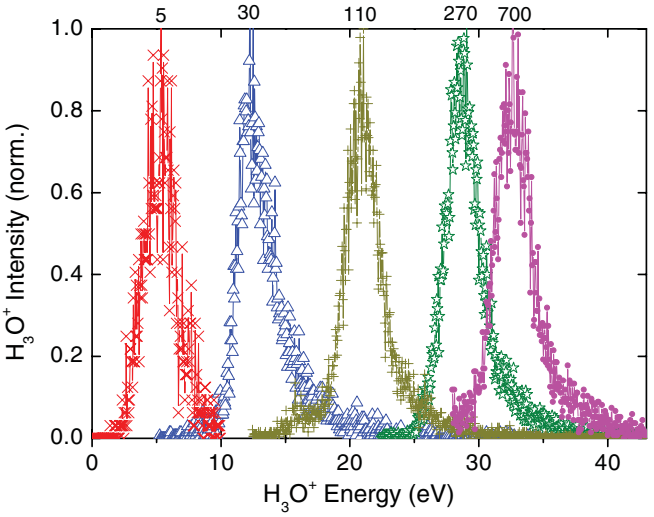

FIG. 1. (Color online) Evolution of the energy distribution of the sputtered H_3O^+ flux from a 1250-ML ice film at 80 K irradiated with 100 keV Ar ions at an ion flux of $j = 3.1 \times 10^{10}$ cm^{-2} s^{-1}. The labels near the peaks are the seconds from the beginning of irradiation for each energy scan.

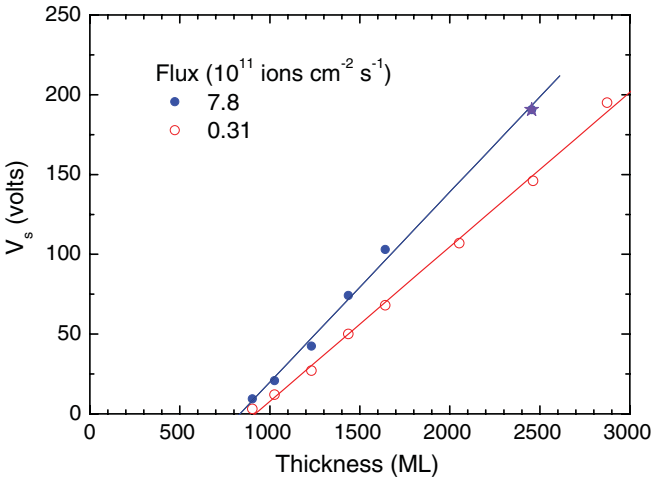

FIG. 2. (Color online) Thickness dependence of surface potential V_s for ice films grown and irradiated at 80 K with 100 keV Ar^+ at fluxes of 0.31 and 7.8 $\times$ 10^{11} cm^{-2} s^{-1}. The datum shown as a star indicate the maximum voltage under breakdown conditions.

energy increases with ion fluence due to charging of the sample.[3]

The energy of the sputtered ions E_p results from an intrinsic value E_0 (5 $\pm$ 1 eV) plus the energy gained by acceleration from the surface potential, V_s to the spectrometer at ground, plus a work function correction, which we neglect here. We used the peak energy of the H_3O^+ energy distribution to get E_p and the average surface potential $V_s = -(E_p - E_0)/e$.

We also measured the surface potential with a KP Technology Kelvin Probe, which allows nondestructive, continuous measurements. This technique has been used previously to study the charging of insulators under stationary electron beams in scanning electron microscopes (SEM),[11] where charges might be trapped at either preexisting or irradiation-induced defects. The Kelvin probe is a noncontact vibrating capacitor device, with a tip probe vibrating at a distance ~2 mm from the ice surface, which measures the potential difference of the surface with respect to the reference probe. The controller of the Kelvin probe adjusts the tip voltage while measuring the displacement current induced by the change of capacitance and obtains the null condition from the analysis of the current-vs-voltage curves.

III. RESULTS

Our measurements show an asymptotic buildup of V_s to a positive saturation value during irradiation due to the accumulation of injected positive charge from the ions. If there was no leakage to ground, the film potential would grow to the ion acceleration voltage, but this is not what we observe. Rather, the charges drift into the substrate, assisted by internal electric fields during irradiation, limiting the surface potential to an equilibrium value. In this condition, the leakage current to the substrate equals the incident ion beam current. The leakage current is a function of film thickness and the mobility of transient trapped charges in the ice, resulting in an energy, temperature, and film thickness dependence of V_s, as described in detail below.

A. Thickness dependence and dielectric breakdown

Figure 2 shows the thickness dependence of the saturation V_s at two different Ar^+ ion fluxes at 80 K. The surface voltage rises linearly with thickness for the higher fluxes used [$V_s = (0.12 \pm 0.1)\ (L - L_0)$ V/ML], with $L_0 = 880 \pm 10$ ML, which exceeds the ionization range of 100 keV Ar^+. Here, L_0 obtained through an extrapolation of the thickness dependence is overestimated, considering that an initial nonlinear dependence should result due to the straggling of ionization range (~1/3 of the penetration depth) which will reach the gold substrate prior to the majority of the deposited charges, at thicknesses between the average ionization range (~600 ML) and L_0 (~880 ML).

In thick films, we observed an erratic behavior of the surface potential in some experiments, with transient drops at high fluences due to sudden dielectric breakdown of the films (Fig. 3, in Ref. 3). The onset of breakdown was unpredictable, e.g. we observed the phenomenon for ~1800 ML films irradiated by 100 keV ions at a flux $j = 7.8 \times 10^{11}$ cm^{-2}s^{-1} but not at $j = 3.1 \times 10^{10}$ cm^{-2}s^{-1} even for thicknesses up to 2900 ML.

B. Energy dependence—Effective thickness

As shown in Fig. 2, films thinner than the maximum projectile range do not charge, thereby demonstrating that the extra positive charges are mobile in the ionization track of the projectile. The charges settle at the end of the ionization range rather than close to the surface, where they are initially deposited, because this condition minimizes the potential energy of image charges.[3]

We further tested this concept by performing experiments at several projectile energies, which result in different implantation depths. The results are shown in Fig. 3 for 1250-ML ice films grown and irradiated at 80 K with a flux of

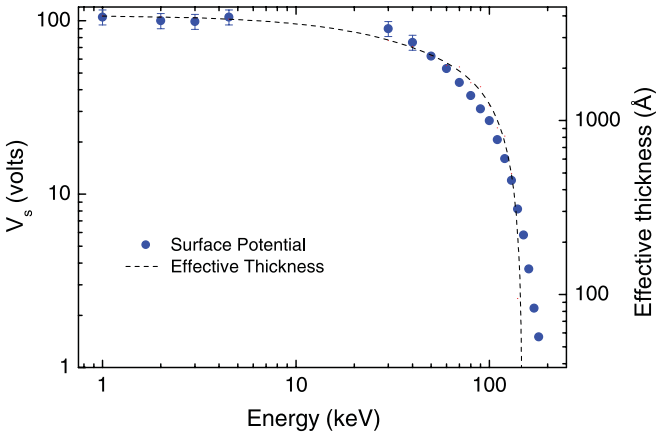

FIG. 3. (Color online) Energy dependence of the surface voltage of 1250-ML ice films irradiated with 1−200-keV Ar ions. The growth and irradiation temperatures were 80 K and the ion fluxes used were 1.1×10^{12} cm^{-2} s^{-1}. The dashed line is the effective thickness = thickness-penetration depth calculated from TRIM.

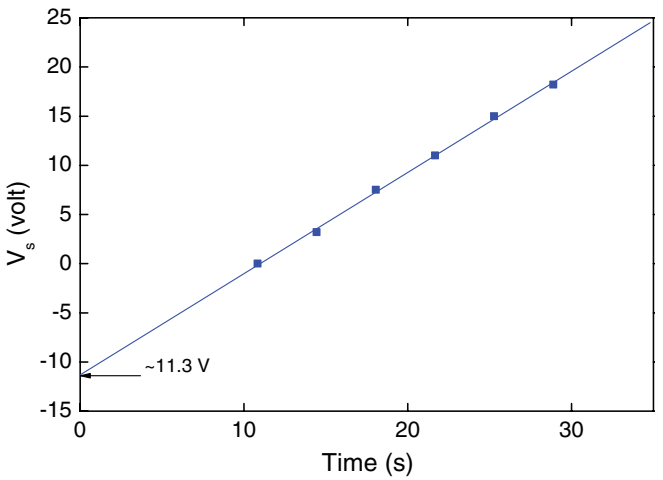

FIG. 4. (Color online) Initial surface voltage indicated by extrapolation of energies vs time of sputtered H_3O^+ from a 2500-ML ice film grown and irradiated at 40 K with a flux of 3×10^{10} Ar^+ cm^{-2} s^{-1}. An extrapolation of V_s to zero time (fluence) gives $V_s(0) = -11.3$ V. The same value was obtained when using other proton energies.

1.1×10^{12} cm^{-2}s^{-1} Ar^+ at energies between 1 and 200 keV. We notice that the surface potential decreases as the penetration range of Ar^+ deepens (approximately proportional to its energy) and becomes negligible when the ion penetration depth is comparable to or larger than the film thickness (Fig. 3). A calculation of the ionization range of 100-keV Ar^+ in water ice with 45° ion angle of incidence using TRIM[10] shows that, due to straggling of the ions, the maximum ionization range will reach the gold substrate when the Ar^+ energy is greater than ∼110 keV, resulting in a nonlinear dependence of the surface potential on film thicknesses (see next section).

C. Initial surface potential

The initial time evolution of the charge of 2500-ML amorphous ice films grown between 15 and 80 K and irradiated with $j = 3.1 \times 10^{10}$ cm^{-2} s^{-1} is shown in Fig. 4. Strikingly, the secondary ion signal did not appear initially but required an incubation time.[3] However, in another experiment where the substrate was biased at +15 V, the secondary ions appeared as soon as the ion beam hit the surface. For a grounded substrate, extrapolation of V_s to zero fluence gives an average negative surface potential of $V_s(0) = -11.3 \pm 2.4$ V, at 40 K. This is close to the value of ∼−8 V in studies with unirradiated ice films, which was attributed to ferroelectricity.[12]

We measured the growth temperature dependence of $V_s(0)$ for 2500-ML ice films between 15 and 80 K and found that the magnitude of this initial voltage decreases with temperature, as shown in Fig. 5. We note that $V_s(0)$ obtained from kinetic energies of protonated water and from measurement with the Kelvin probe are the same and also consistent with previously published measurements on ice films of our thickness.[12]

D. Effect of irradiation temperature

We measured the temperature dependence of charging of crystalline ice by (i) depositing a film at 140 K, (ii) cooling in steps from 140 to 20 K, and then (iii) warming again in steps back to 140 K. At each step, we held the ice temperature constant and irradiated with a flux of 3.1×10^{10} cm^{-2} s^{-1} until the maximum surface voltage was achieved (requiring a time scale from <1 to ∼200 s). Without irradiation, charge drift into the substrate reduced the surface voltage, as seen in the decrease of secondary ion energy between the end of irradiation and its resumption at the next temperature step. The value of the starting V_s at each temperature depends on the time since last irradiation and the temperature-assisted relaxation rate. Figure 6 shows that V_s is maximum at low temperatures and falls rapidly above 100 K, becoming negligible at 140 K.

We performed a similar measurement on amorphous ice deposited at 15 K, which we continuously warmed to 158 K, and then cooled back to 15 K, under constant irradiation with 100 keV Ar^+. In contrast to crystalline ice, the amorphous sample exhibited a hysteresis due to annealing of defects upon crystallization above 135 K.

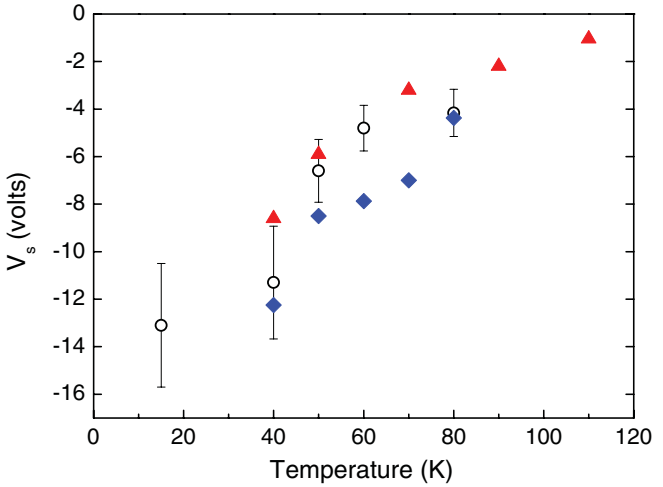

FIG. 5. (Color online) The dependence of the initial V_s for 2500-ML ice films on growth temperature. Diamonds: Kelvin probe data; circles: SIMS data, triangles: data from Ref. 11, adjusted by thickness.

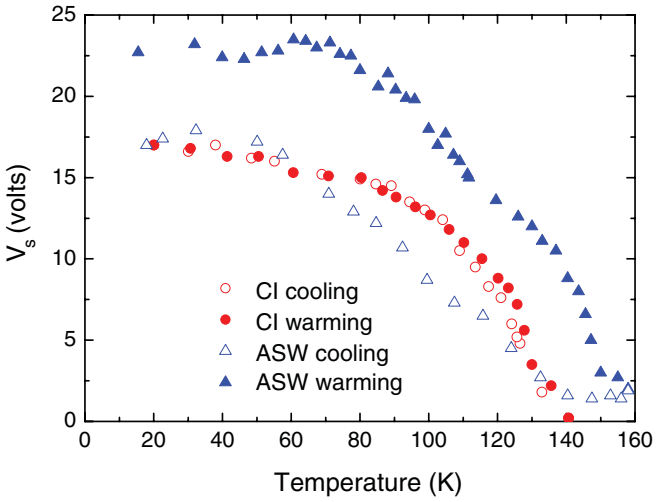

FIG. 6. (Color online) Temperature dependence of the surface potential of a 1250-ML crystalline ice (CI) film grown at 140 K, during cooling (open circles) from 140 to 20 K, and then during warming (solid circles) back to 140 K. The triangles are the data for a 1250-ML ice film of amorphous solid water (ASW) grown at 20 K during warming (closed triangles) from 20 to 158 K and then cooling (open triangles) back to 20 K. At each temperature, the ice film was charged to its saturation state with 100 keV Ar^+ at a flux of 3.1×10^{10} cm^{-2} s^{-1}.

E. Discharging

In several experiments, we turned off the ion beam after equilibration of the surface charge and then measured the decay over time of the film voltage by monitoring the decreasing secondary ion energies. To avoid significantly affecting the charge, each measurement was made using very low fluences ($<10^{11}$ cm^{-2} during brief 2−3-s ion beam exposures). The normalized discharging curves of two films of different thickness (1400 and 2500 ML) are plotted in Fig. 7. We also used the Kelvin probe to monitor the surface potential of a 1250-ML ice film grown at 80 K and charged at 40, 60, and 80 K (Fig. 7). We note that the discharging curves measured from the secondary ion energies using SIMS agree with those measured with the Kelvin probe.

The data in Fig. 7 show two distinct discharging regimes, a fast one below ∼500 s that is independent of temperature and a much slower decay at longer times, which depends on temperature. The simplest description of the data is obtained by a double exponential decay function:

$$\frac{V_s(t)}{V_s(0)} = f_1 \exp[-t/\tau_1] + f_2 \exp[-t/\tau_2]. \quad (1)$$

Fits give $f_1/f_2 \approx 1/3$ for all 5 curves. Here, τ_1 and τ_2 are time constants, and τ_2 depends on temperature.

The discharging curves were the same within errors for films of different thicknesses. However, while $\tau_1 \approx 600$ s and does not exhibit a temperature dependence, τ_2 decreases with temperature: $\tau_2 \approx 18$, 9, and 4×10^4 s for 40, 60, and 80 K, respectively. This phenomenon is discussed below.

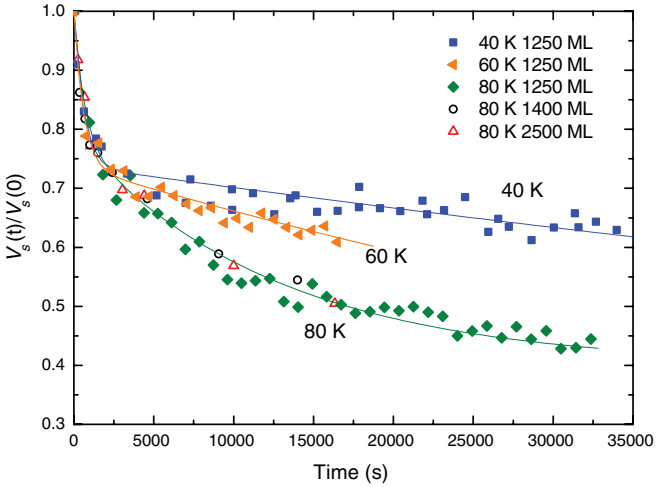

FIG. 7. (Color online) Discharging curves for a 2500-ML ice film grown at 80 K. Open symbols: measured with SIMS; closed symbols: measured with Kelvin probe. All curves are fitted with the double exponential Eq. (19).

IV. DISCUSSION

As a basis for our analysis, we further develop the simple model proposed in our previous paper.[3] The first stage of this model is the formation of an ionization track by the projectiles, extending from the surface to close to the final penetration depth. The track will consist mainly of electrons and positive ions (e.g. H^+, OH^+). A short time (several μs) after the ionization track neutralizes by electron-ion recombination, the extra charge injected by the ion will be at the end of the ionization range, as shown by the linear dependence of V_s on effective thickness. The potential energy is minimized in this configuration because the deposited charge is as close as possible to its image at the substrate.

The nature of the excess charge is not known from this or other experiments on radiation effects in ice, but it is likely a hydronium ion, H_3O^+, formed by solvation of a proton which becomes trapped. The binding energy of this trapped ion will depend on the configuration, including the presence of defects. In principle, a continuum of binding energies are possible, but the double-exponential decay in Fig. 7 suggests that the trap states can be grouped in two distinct categories, shallow and deep traps, rather than in a continuum. Such a simple two-state charge trapping model has been used successfully in polymeric materials.[13]

Thus, in this heuristic model, we assume that the injecting charges will reside in either shallow traps or deep traps with column integrated number densities q_S and q_D, at the time of deposition. Detrapping of the ions can occur by local thermal fluctuations assisted by the electric field (Poole–Frenkel mechanism). The charges will eventually drift to the substrate at a rate characterized (in the presence of irradiation) by time constants of τ_s^j and τ_d^j, from the end of the ionization range. The lifetimes τ_s^j andτ_d^j correspond to detrapping from shallow and deep traps, respectively. Since we do not observe any film thickness dependence of discharging, we assume that the detrapped charges q_s and q_d flow freely into the substrate without being trapped again and without intertrap transfer.

With these simplified considerations, we propose the following equation to describe the evolution of charge density during irradiation with ion flux j:

$$q = q_s + q_d, \tag{2}$$

$$\frac{dq_s}{dt} = js - \frac{q_s}{\tau_s^j}, \tag{3}$$

$$\frac{dq_d}{dt} = jd - \frac{q_d}{\tau_d^j}, \tag{4}$$

$$s + d = 1, \tag{5}$$

where s and d are the probabilities for trapping of charges in shallow and deep traps. Here, we do not consider the contribution from secondary electron emission, since the effect quickly becomes negligible as V_s exceeds a few volts positive. The solution for Eqs. (2)–(5), considering initial conditions $q_s(0) = 0$ and $q_d(0) = 0$, is

$$q = q_s + q_d = js\tau_S^j\left[1 - \exp\left(-\frac{t}{\tau_s^j}\right)\right] + jd\tau_d^j\left[1 - \exp\left(-\frac{t}{\tau_d^j}\right)\right], \tag{6}$$

where we have neglected the contribution of the initial negative surface voltage upon deposition, which is a small effect for our relatively thin films (see Ref. 7 for a discussion of the thickness dependence). By Gauss's theorem, assuming q_S and q_D are located near the end of the ionization range, the surface potential is

$$V_s = \frac{e}{\varepsilon_0\varepsilon_r}\int_0^L q dx, \tag{7}$$

$$V_s = \frac{eLj}{\varepsilon_0\varepsilon_r}\left\{s\tau_S^j\left[1 - \exp\left(-\frac{F}{j\tau_s^j}\right)\right] + d\tau_d^j\left[1 - \exp\left(-\frac{F}{j\tau_d^j}\right)\right]\right\}, \tag{8}$$

where $F = jt$ is the ion fluence, L is the distance of between the substrate and the location of the trapped charges (end of the ionization track), and $\varepsilon = \varepsilon_0\varepsilon_r$ is the static permittivity of water ice [$\varepsilon_r = 3$ (Ref. 14)]. Here, L depends on ion energy through the ionization range plus its straggling.

Detrapping of the charge q_s and q_d assisted by the average electric field (negligible from the film surface down to the ion range) appears unimportant, since the charging time constants do not depend on fluence.[3] On the other hand, local fields that exceed a critical value may detrap q_s and q_d. Such a critical field can be produced by a projectile or a secondary electron colliding with a trapped charge by passing within a critical radius $r_{c,i}$,[3] where $i = s, d$. The trapping time will be given by $\tau_c = 1/\sigma_i j$, where σ_i is the collisional detrapping cross section determined by $\sigma_i = \pi r_{c,i}^2$. Thus τ_s^j and τ_d^j can be written as

$$\left(\tau_s^j\right)^{-1} = \sigma_s j + (\tau_s)^{-1}, \tag{9}$$

$$\left(\tau_d^j\right)^{-1} = \sigma_d j + (\tau_d)^{-1}, \tag{10}$$

where τ_s and τ_d are the thermal detrapping time constants in the absence of ion irradiation. Replacing τ_s^j and τ_d^j in Eq. (8), we obtain, at saturation fluences,

$$V_s(F \to \infty) = \frac{eLj}{\varepsilon}\left(s\tau_s^j + d\tau_d^j\right) = \frac{eLj}{\varepsilon}\left[\frac{s}{\sigma_s j + 1/\tau_s} + \frac{d}{\sigma_d j + 1/\tau_d}\right]. \tag{11}$$

Under the limit for high fluxes, where j is much larger than $1/\sigma_s\tau_s$ and $1/\sigma_d\tau_d$, which applies to our experiments:

$$V_s(F \to \infty, j \to \infty) = \frac{eL}{\varepsilon}\left(\frac{s}{\sigma_s} + \frac{d}{\sigma_d}\right), \tag{12}$$

independent of flux. In our previous paper,[3] we found charging to be described by a single exponential with a time constant $\tau_0 = 150 \pm 30$ s at $j = 3.1 \times 10^{10}$ cm^{-2} and at 80 K. This time constant is much shorter than τ_s and τ_d (called τ_1 and τ_2 in Fig. 7); thus the ion irradiation induced detrapping process dominates, and $(\tau_i)^{-1}$ in Eqs. (9) and (10) can be neglected. A single exponential function can be obtained by assuming that collisional detrapping is the same for shallow and deep traps, $\sigma_s \approx \sigma_d$, which may be due to scrambling of defect sites during irradiation. Thus, using the values of τ_0 and j given above, $\sigma_i \approx 1/j\tau_0 \sim 2.2 \times 10^{-13}$ cm^2, and $r_{c,i} \approx 26$ Å. At this distance, the local electrical field generated by an elementary charge e is

$$E_{\text{local}} = \frac{e}{4\pi\varepsilon_o\varepsilon_r r_{c,i}^2} = 7 \times 10^7 \text{V/m}. \tag{13}$$

This field is reasonable for field ionization of a charge trapped at an atomic size.

With the above assumption $\sigma_s \approx \sigma_d$, $\tau_d^j = \tau_s^j$ at the high fluxes used in our experiments, and Eq. (8) reduces to:

$$V_s = V_\infty\left[1 - \exp\left(-F/j\tau_s^j\right)\right] = V_\infty(1 - \exp\{-F[\sigma_s + (\tau_s j)^{-1}]\}), \tag{14}$$

$$V_\infty = \frac{eLj\tau_s^j}{\varepsilon} = \frac{eL\varepsilon^{-1}}{\sigma_s + (\tau_s j)^{-1}}, \tag{15}$$

that is, a single exponential growth as in our previous simpler model.[3] However, if the ion flux were much lower than those used in the experiments, so that collisional detrapping does not dominate the time constant, charging would depend on flux and be described by a double exponential curve.

During discharging, $j = 0$, and Eqs. (3) and (4) become:

$$\frac{dq_s}{dt} = -\frac{q_s}{\tau_s}, \tag{16}$$

$$\frac{dq_d}{dt} = -\frac{q_d}{\tau_d}. \tag{17}$$

Therefore,

$$q = q_S(0)\exp\left(-\frac{t}{\tau_S}\right) + q_D(0)\exp\left(-\frac{t}{\tau_D}\right), \tag{18}$$

and, accordingly,

$$V_s = V_1(0)\exp\left(-\frac{t}{\tau_s}\right) + V_2(0)\exp\left(-\frac{t}{\tau_d}\right), \tag{19}$$

where $t = 0$ is the time at which the ion beam is turned off, and $V_1(0) = \frac{eLsj\tau_s}{\varepsilon}$ and $V_2(0) = \frac{eLdj\tau_d}{\varepsilon}$ are the components of the surface potential caused by the charges initially trapped in shallow and deep traps, respectively.

We used Eq. (19) to fit the discharge curves in Fig. 7 with $\tau_s = \tau_1$ and $\tau_d = \tau_2$. The time constant τ_s was given above from fitting of the discharging curves measured at 40, 60, and 80 K (Fig. 7): $\tau_s = 600 \pm 200$ s, consistent with 900 ± 300 s given in our previous paper,[3] where the measurement time scales were such that τ_d was not important. The value of τ_s is within the range of 100−1000 s calculated for the dielectric relaxation time of low-density amorphous ice at 130 K.[15] In contrast, as shown in Fig. 7, the values of τ_D are above 40 000 s and depend strongly on temperature. From the fit of Eq. (19) (Fig. 7), we find that $s/d \approx 100$, 50, and 22 at temperatures of 40, 60, and 80 K, respectively, and a ratio $s\tau_s/d\tau_d \approx 0.33$ of shallow to deep trap densities with no discernable temperature dependence. The very slow decay above 40 000 s and its temperature dependence indicate a thermally assisted Poole–Frenkel mechanism. This can be detrapping of the ion or detrapping of a trapped electron into the conduction band that can then neutralize the ion. The depth of the traps can be estimated from an Arrhenius plot; since we have only three temperatures, we can only give an approximate value, ∼0.006 eV.

V. SUMMARY

Charging of ice on a conducting substrate requires that the projectile ions are stopped in the ice and that the ice temperature is below 160 K. Before the occurrence of dielectric breakdown, the linear dependence of the surface voltage over film thickness is consistent with that over incident ion energy. Freshly deposited ice films exhibit (before ion irradiation) negative surface potentials, consistent with previously published observations of ferroelectricity in ice.

Discharging of ice is determined by two time constants, a shorter one that does not depend on temperature (τ_s) and a much longer, temperature-dependent one, assigned to thermal detrapping time from deep traps, τ_d. Amorphous ice films were charged to a higher surface potential compared to crystalline ice films under the same conditions. An analytical model successfully explains the charging and discharging processes.

ACKNOWLEDGMENT

This research was supported by Grant AST0807830 from the National Science Foundation.

*Corresponding author: Dr. Raúl Antonio Baragiola, Engineering Physics, Thornton Hall, University of Virginia, Charlottesville, VA 22904-4238; raul@virginia.edu

[1] M. G. Kivelson, K. K. Khurana, D. J. Stevenson, L. Bennett, S. Joy, C. T. Russell, R. J. Walker, C. Zimmer, and C. Polanskey, J. Geophys. Res. **104**, 4609 (1999).

[2] M. Famá, B. D. Teolis, D. A. Bahr, and R. A. Baragiola, Phys. Rev. B **75**, 100101 (2007).

[3] J. Shi, M. Famá, B. D. Teolis, and R. A. Baragiola, Nucl. Instr. Meth. Phys. Res. B **268**, 2888 (2010).

[4] W. C. Simpson, T. M. Orlando, L. Parenteau, K. Nagesha, and L. Sanche, J. Chem. Phys. **108**, 5027 (1998).

[5] R. Balog, P. Cicman, D. Field, L. Feketeov, K. Hoydalsvik, N. C. Jones, T. A. Field, and J. P. Ziesel, J. Phys. Chem. A **115**, 6820 (2011).

[6] R. A. Baragiola, M. Shi, R. A. Vidal, and C. A. Dukes, Phys. Rev. B **58**, 13212 (1998).

[7] D. E. Grosjean, R. A. Baragiola, and W. L. Brown, Nucl. Instr. Meth. Phys. Res. B **157**, 116 (1999).

[8] D. E. Grosjean, R. A. Baragiola, and W. L. Brown, Nucl. Instr. Meth. Phys. Res. B **164-165**, 891 (2000).

[9] N. J. Sack and R. A. Baragiola, Phys. Rev. B **48**, 9973 (1993).

[10] J. F. Ziegler and J. P. Biersack, TRIM 2008 available at srim.org.

[11] M. A. Stevens-Kalceff, Microscopy and Microanalysis **10**, 797 (2004).

[12] M. J. Iedema, M. J. Dresser, D. L. Doering, J. B. Rowland, W. P. Hess, A. A. Tsekouras, and J. P. Cowin, J. Phys. Chem. **102**, 9203 (1998).

[13] G. Chen and Z. Xu, J. Appl. Phys. **106**, 123707 (2009).

[14] H. F. Wang, R. C. Bell, M. J. Iedema, G. K. Schenter, K. Wu, and J. P. Cowin, J. Phys. Chem. B, **112**, 6379 (2008).

[15] K. Kutzner, Thin Solid Films **14**, 49 (1972).